What Criteria Define an Ideal Skeletonisation Reference in Object Point Clouds?[*]

Qingmeng Wen[1][0000−0002−8972−4042], Seyed Amir Tafrishi[1][0000−0001−9829−3144], Ze Ji[1][0000−0002−8968−9902], and Yu-Kun Lai[2][0000−0002−2094−5680]

[1] School of Engineering, Cardiff University, CF24 3AA, UK
{wen1, tafrishisa, jiz1}@cardiff.ac.uk
[2] School of Computer Science and Informatics, Cardiff University, CF24 4AG, UK.
laiy4@cardiff.ac.uk

Abstract. The skeletonisation methods of 3D object models gained noteworthy attention in recent years and have been extensively investigated, inspired by their wide-range applications, including computer graphics and robotics. However, there remains a gap that the quantitative reference of high-quality skeletonisation results is hardly given by the previous studies. Building upon previous research on point cloud skeletonisation, this paper explores the inherent characteristics of the skeletonisation process across objects of varying shapes. This analysis aims to provide intuitive insights into the quality of the resulting desirable skeletons. Additionally, we introduce a new concept of stable convergence of contraction based on distributions of geometric curvature and vectorial normal changes.

Keywords: Reference skeleton · Point cloud · Computer vision · Geometric methods

1 Introduction

The skeleton of a shape is a contracted and medial structure that intuitively represents the shape both topologically and geometrically [23]. For 3D shapes captured from point clouds, there are two known shape skeletons, the medial surface and curve skeletons. Accordingly, skeletonisation is the process that generates the desirable skeletal descriptors of the object model by a set of computations [8]. This skeletonisation technique is highly valuable for robotics applications, ranging from object reconstruction and manipulation [25, 27] to localization and navigation [8, 19]. Although the algorithms for skeletonisation from point clouds have been extensively researched by previous studies, quantitative analysis of desirable skeleton is rarely found [23], and there has been no approach to understanding the contraction convergence state from a control theory point of view.

As for the medial surface, either by simplifying Delaunay triangulation or computing a number of balls, the medial axis transform (MAT) can be estimated

---

with the information of Voronoi diagram [1, 2]. Chazal et al. [6] proposed λ axis transform that is calculated by estimating the center point sets of the maximal inscribed sphere. Extended by Giesen et al. [10], a scale factor is used to generate MAT with fewer irrelevant spikes. In addition, the surface skeleton, obtained through Laplacian-based contraction (LBC) applied to either a point cloud or a mesh model, serves as an alternative approximation of the medial surface [4, 5]. In recent years, the learning-based method has been applied to predict the "skeletal mesh" of the shapes [12]. While the medial surface faithfully corresponds to the original shape with intricate structure, the curve skeleton offers a more simplified representation that facilitates modeling and manipulation [5, 9, 23].

Due to its simplicity and versatile applications, curve skeletons have attracted significant interest from researchers. The rotational symmetry axis (ROSA) is defined by a set of geometric centers of cross-section points, achieved through the design of an optimal "cutting plane". [24]. Huang et al. [11] considered the L1-medians as the pivotal points of the skeletons, resulting in accurate 1D curves. Derived from the idea of curve skeletonisation from meshes [4], Cao et al. [5] abstract the curve skeleton from contracted point clouds with a Laplacian-based contraction (LBC) method. Based on this, our previous work reduces the computation cost of LBC by an in-loop local point cloud reduction strategy [26]. Besides, Wu et al. [28] adopted the resampling strategy to calibrate the resultant skeleton from LBC to refine the skeletons of maize plants. In a recent study by Meyer et al. [13], the quality of Laplacian-based contraction (LBC) applied to cherry tree point clouds is enhanced by discriminatively weighting the Laplacian matrix, taking into account the semantic segmentation of the points.

The application of curve skeletons might cover many areas, including virtual navigation, computer graphics, medical imaging, and more [7, 20, 23]. Recent studies suggest that curve skeletons hold promise for advancements in robotic research. Given that topological connections often encapsulate the essential structure of objects with hole-like features, researchers have begun applying topological curves in the planning of grasps for such objects [14, 22]. As argued by Przybylski et al. [15–17], the excellent geometrical representations of shapes may contribute to aiding robots in planning stable grasps. Besides, through the design of a tailored grasping strategy, it has been demonstrated that curve skeletons can be effectively utilized for efficient and high-quality grasping planning [25].

The evaluation of skeletonisation methods is of significant importance to the validation of applicability. However, evaluating and validating the shape skeletonisation results remains a challenging task. Most works on skeletonisation simply discussed their experimental results by visually comparing resultant skeletons [4, 11, 18]. As for the remaining quantitative analysis, Arcelli et al. [3] compared the results with recoverabilities. Sobiecki et al. [21] gave the definition of "centeredness" of various types of skeletons to evaluate skeletonisation performance. Comparing resultant skeletons with ground truth is one approach, but establishing a universally accepted definition of the ground truth presents another challenging issue [13]. Currently, defining what constitutes a high-quality skeleton remains a significant challenge [20, 23]. However, the evaluation of skele-
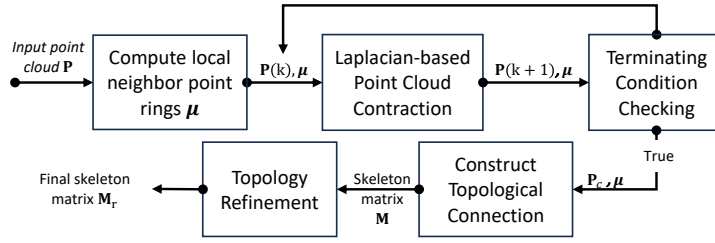
Fig. 1: General structure of Laplacian-based contraction of point clouds

tonisation results is indeed crucial for advancing the field, particularly in terms of its practical applications.

Based on the previous work, this paper investigates the geometrical properties of Laplacian-based contraction and the quality of the resultant skeleton. Firstly, the methodology of evaluation metrics and the definition of the high-quality skeleton is discussed in Section 2. In Section 3, we demonstrate our experimental results and observations. Lastly, we conclude our work in Section 4.

2 Methodology

In this section, we will looking into the meaningful geometrical properties of stable contraction and skeletonisation, addressing the challenge of evaluating the skeletonisation results, after the brief introduction of Laplacian-based skeletonisation (LBC).

2.1 Overview of Laplacian-based skeletonisation

The Laplacian-based skeletonisation is a pipeline that abstracts the skeleton vertices and connections from the points contracted by Laplacian weights. The Laplacian-based skeletonisation pipeline generally consists of 4 processes as illustrated in Fig. 1.

Given an input point cloud $\mathbf{P} \in \mathbb{R}^{n \times 3}$, the pipeline starts with computing the point-wise neighbour-rings of the point cloud. For each point, its neighbour points can be queried by the k-nearest neighbours (KNN) algorithm. After obtaining the Delaunay triangulation of the neighbor points, the dimensions of the neighbor point coordinates data are reduced to 2D using Principal Component Analysis (PCA), and the ring points of the anchor point are derived from the triangulation results.

With the information of neighbour ring points, the Laplacian matrix $\mathbf{L} \in \mathbb{R}^{n \times n}$ is defined as

$$L_{ij} = \begin{cases} \omega_{ij} = \cot \alpha_{ij} + \cot \beta_{ij}, & \text{if } \mathbf{p}_j \in \boldsymbol{\mu}_i; \\ \sum_{k \in \boldsymbol{\mu}_i}^{k} -\omega_{ik}, & \text{if } i = j; \\ 0, & \text{Otherwise; ,} \end{cases} \quad (1)$$

where $\boldsymbol{\mu}_i$ ring point set of set of point $\mathbf{p}_i$, and α_{ij} and β_{ij} are two opposite angles of edge (i,j) in triangles of the point ring. Following that, the contracted cloud points in iteration $k+1$ can be obtained by solving the system below

$$\begin{bmatrix} \mathbf{W}_L\mathbf{L} \\ \mathbf{W}_H \end{bmatrix} \mathbf{P}_{k+1} = \begin{bmatrix} \mathbf{0} \\ \mathbf{W}_H\mathbf{P}_k \end{bmatrix}, \tag{2}$$

where $\mathbf{W}_L, \mathbf{W}_H \in \mathbb{R}^{n \times n}$ are contraction and attraction weights respectively. The contraction weights and the attraction weights work jointly to balance the process of pushing the points toward the medial axis. Please note, $\mathbf{W}_L, \mathbf{W}_H$ must be updated after each iteration to make sure the contraction process continues [5]. The contraction process in the pipeline runs iteratively until the resultant point clouds meet the terminating condition. The terminating condition can be defined either based on global feature or the local feature of the cloud points [5, 26].

After the contraction process, the approximation of the medial surface, comprised of the contracted point set known as the surface skeleton, is obtained. This surface skeleton can be abstracted to skeleton vertices using farthest point sampling. The connections among different vertices are derived from the point-wise neighbor ring information. Lastly, the final skeleton is acquired after necessary refinement.

2.2 Characteristics of the stable contraction & skeletonisation

Although Laplacian-based contraction can generate both the surface skeleton and the final curve skeleton, evaluating the quality of the resultant skeleton remains a considerable challenge. To investigate the characteristics of stable contraction, we examine deformation and distortion induced by the Laplacian contraction process by analysing the changes in surface normal vectors and curvatures.

To calculating distances among the surface normal vectors, the cosine similarity is chosen for measuring the similarity. Compared to other metrics, the cosine similarity is more indicative of the directions [30]. The general definition for m-dimensional vectors $\mathbf{n}_x$ and $\mathbf{n}_y$ is given by

$$S_C(\mathbf{n}_x, \mathbf{n}_y) = \cos(\theta) = \frac{\mathbf{n}_x \cdot \mathbf{n}_y}{\|\mathbf{n}_x\|\|\mathbf{n}_y\|} = \frac{\sum_{i=1}^m n_{x,i} n_{y,i}}{\sqrt{\sum_{i=1}^m n_{x,i}^2}\sqrt{\sum_{i=1}^m n_{y,i}^2}}, \tag{3}$$

where θ is the included angle between $\mathbf{n}_x$ and $\mathbf{n}_y$. Since the range of the cosine function is nonlinear to the angle, the cosine distance is normalised by

$$D_\theta = \frac{\arccos(S_C)}{\pi}, \tag{4}$$

where D_θ is the normalised angular distance, and $0 < D_\theta < 1$. For each point $\mathbf{p}_i$, we compute the distance of the normal vectors between the original and the

contracted point cloud using

$$D_{\theta,k,i} = \frac{\arccos(S_C(n_{k,i}, n_{0,i}))}{\pi},$$ (5)

where $n_i(k), n_i(0)$ are normal vectors of the point of the original positions and the new positions after k-th contraction iteration, respectively. As illustrated in Eq. (5), the normal vectors are required before computing their distance. Similar to computing local neighbor rings, a number of nearest neighbor points around each cloud point are used for normal vector estimation. This is achieved by calculating the covariance matrix $\mathbf{C}$ of the neighbor points, defined by

$$\mathbf{C} = \frac{1}{n} \sum_{i=1}^{n} (\mathbf{p}_i - \mathbf{c})(\mathbf{p}_i - \mathbf{c})T,$$ (6)

where n is the number of the neighbours used for estimation, $\mathbf{c}, \mathbf{p}_i$ are the coordinates of the anchor point and its corresponding i-th closest neighbour point, respectively. After calculating the eigenvectors $\mathbf{v}_1$, $\mathbf{v}_2$, $\mathbf{v}_3$ and the corresponding eigenvalues λ_1, λ_2, λ_3 satisfying $\lambda_1 < \lambda_2 < \lambda_3$ of that covariance matrix, the normal vector of the point is obtained as $\mathbf{v}_1$.

To obtain the curvature differences between the results of contraction and the original point cloud, we define the curvature differences here. With the covariance matrix $\mathbf{C}$ mentioned above, the curvature of the point can be estimated and normalised by

$$\kappa_n = \frac{\lambda_1}{\sum_{i=1}^{3} \lambda_i}.$$ (7)

Since the curvatures are obtained as scalars, we can easily obtain the differences of curvatures between the input point cloud and the contracted one by

$$\Delta\kappa_{n,k} = \kappa_{n,k} - \kappa_{n,0},$$ (8)

where $\kappa_n(k)$ and $\kappa_n(0)$ represent the curvature at the point position after k-th contraction iteration and the original point position, respectively.

Here, we propose a hypothesis on the stable convergence of contraction and outline how it is qualitatively evaluated based on the convergence of the contracted surface. It is important to note that to the best of our knowledge, there has not been research discussing the desirability or stability of convergence of contraction. Thus, these propositions are developed and verified based on the obtained real object results from multiple skeletonisation strategies. Let's assume, we have the original point set $\mathbf{P}_o = \{\mathbf{p}_i\}$ of the object and the contracted point cloud obtained in k-th contraction iteration $\mathbf{P}_k = \{\mathbf{p}_{k,i}\}$. Here, we use i and to denote the i-th point in the point set. The surfaces of the point clouds $\mathbf{P}_o$ and $\mathbf{P}_k$ are denoted as U_o and U_k respectively. The stability of contraction is assessed locally with respect to the boundary region of set points $\mathbf{X}_o \in \mathbf{P}_o$. If the iterative contraction results, denoted as $\mathbf{X}_k \ll \mathbf{P}_k$, satisfy the condition $X_{k+1} < X_k \ll X_o$, where the contracted surface is constrained to $U_{k+1} < U_k \ll U_o$, we define this condition as boundedness to assess the stability
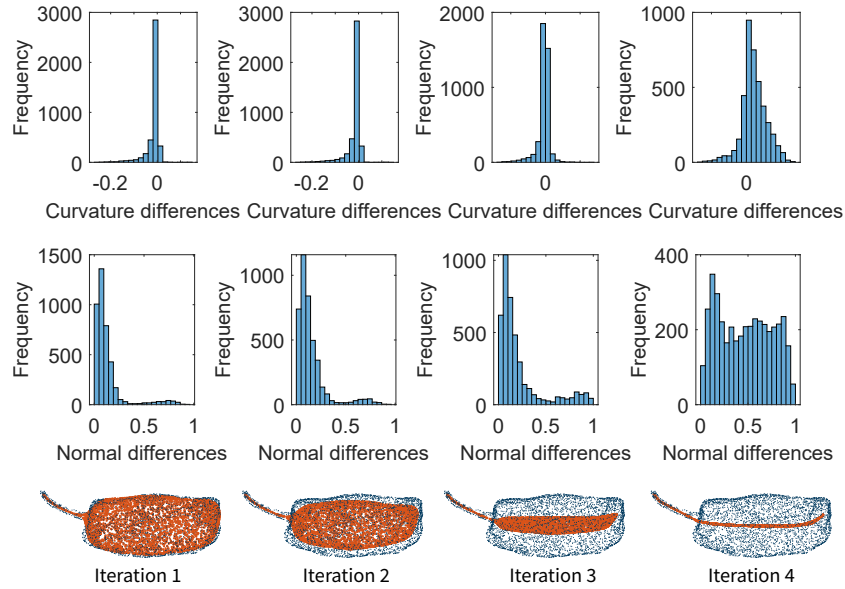
Fig. 2: Changes of normal vector and curvature differences within contraction process.The selected point cloud object is chilli.

of contraction. Besides, the stable contraction convergence is checked through the difference of the curvature $\Delta\kappa_{n,k}$ and the difference of the normal vectors $D_{\theta,k,i}$ at the local surface areas. For the process of point cloud contraction with stable convergence, the distribution of $D_{\theta,k,i}$ and $\Delta\kappa_{n,k}$ are expected to be symmetric and unimodal, resembling "bell shape". Also, the average of $D_{\theta,k,i}$ and $\Delta\kappa_{n,k}$ are expected to converge towards 0.5 and 0 values respectively. Apart from the shared features, the unique pattern of the distribution might indicate the special geometrical structures varying in different types of shapes or unexpected shape handling. Since the contracted results are the approximation of the surface skeleton, that pattern is also applicable for evaluation of the quality of the finalised surface skeleton. Besides, the Laplacian-based curve skeletonisation also relies on stable contraction results. Thus, the stable and converged contraction pattern also contributes to generating high-quality curve skeletons.

3   Results and Discussion

In this section, we will present the observations of normal vector and curvature difference patterns, along with the results of various object skeletonisations. The point cloud models utilized in this section are sourced from the OmniObject3D dataset [29]. The skeletonisation method employed by default is the baseline Laplacian-based skeletonisation [5]. Additionally, we applied our findings to
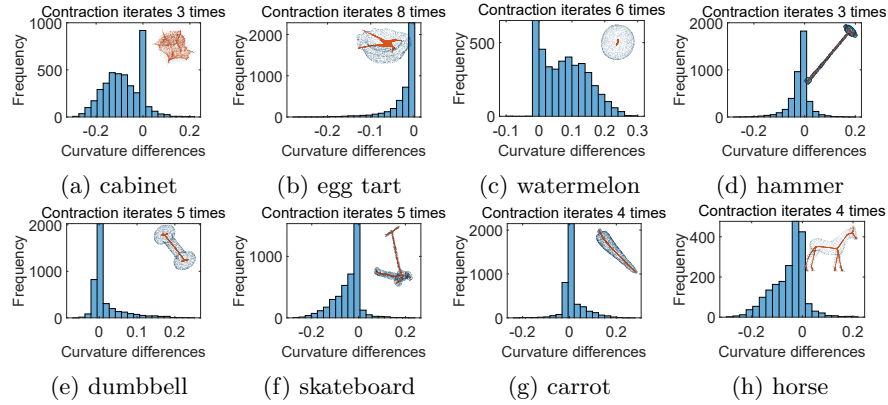
Fig. 3: Curvature differences between the input and point cloud after final contraction. The original point cloud (grey) with the contraction results (red) are put at the top right corner of each histogram
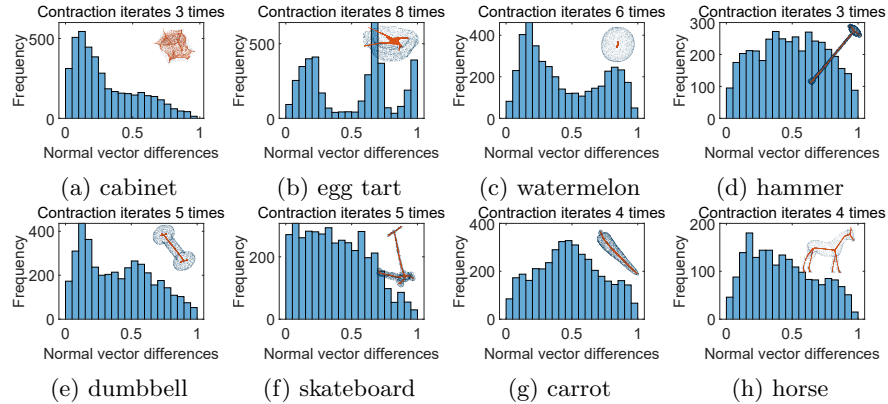
Fig. 4: Normal vector differences between the input and point cloud after final contraction. The original point cloud (grey) with the contraction results (red) are put at the top right corner of each histogram

GLSkeleton [26], a skeletonisation method proposed in our previous work, to validate the hypothesis.

To show the geometrical property changes within the contraction iterations, we generate the histogram of the differences of curvature and the normal vectors between each contraction iteration output and the original point cloud. As illustrated in Fig. 2, the histogram pattern changes demonstrate that the pattern of the curvature differences and the normal vector differences can indicate the geometrical convergence in the contraction process. While the shape of the object is deformed and pushed inward, the pattern of the mentioned geometri-

(a) cabinet   (b) egg tart   (c) watermelon   (d) hammer

(e) dumbbell   (f) skateboard   (g) carrot   (h) horse
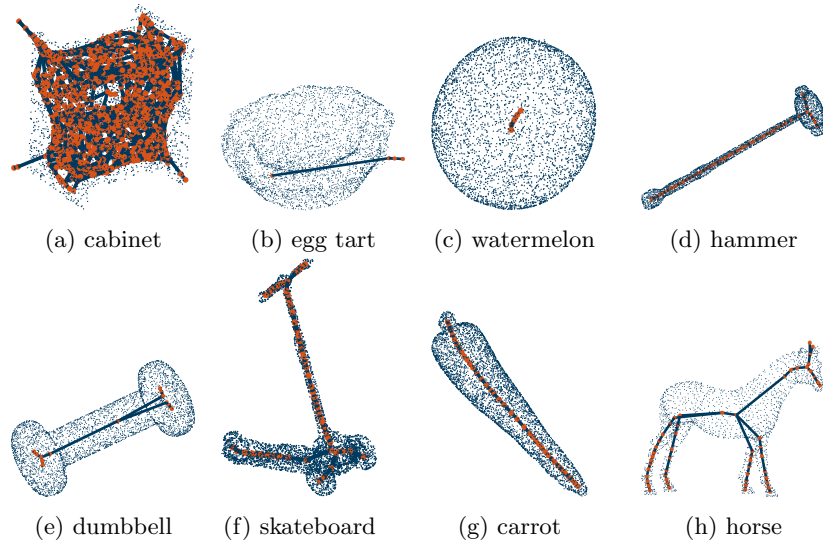
Fig. 5: Resultant curve skeletons

cal characteristics are changed correspondingly along the iterations. Overall. the distribution of differences between the normal vectors and curvatures gradually becomes symmetric during contraction, suggesting stable convergence. As for the curvature differences shown in the first row of Fig. 2, the curvature differences are minimal. Its distribution remains a "bell shape" and the normality of the distribution keeps increasing. It means that the contraction on the curvature aspect converges stably in the whole process. As shown in the second row of Fig. 2, the change of the pattern of the normal vector differences are quite different in comparison with the curvature difference change. The distribution of surface normal vectors differences are skewed left at the beginning, after which the normal vector differences gradually increased and the pattern is approaching a symmetric and unimodal distribution. It means that the contraction process is unstable at the beginning. But with the control of contraction and attraction weights (2) updated in iterations, the distribution is pushed to a stable stage. The changes are also reflected on the shape, which is demonstrated by the third row of the figure. Start with the contracted surface being non-parallel to the original surface and out of the boundary, the surface is gradually pushed inward and forming the surface skeleton at the end.

The assessment of final contraction outcomes relies on a comparative analysis of curvature and normal vectors between the contracted and original point clouds, as illustrated in Figs. 3 - 4. Notably, the contraction outcomes for certain objects, such as the cabinet, egg tart, and watermelon, deviate from the original topology, indicating lower quality. Conversely, other objects exhibit well-contracted forms with distributions that align more closely with the desired stability criteria outlined in Section 2.2.

As for the curvature differences, the distributions for the cabinet, egg tart, and watermelon display either skewed or spiky distributions, with average curvature differences diverging significantly from the expected value of zero. In contrast, the curvature distributions for other objects tend towards a bell-shaped curve centered around zero, indicating better adherence to the original shape.

For the normal vector differences, distributions of those with worse contraction also demonstrate less symmetric histogram patterns. Since the contraction process of the cabinet terminated unexpectedly, the normal vector differences are skewed left. Similarly, the unexpected peak on the left in the histogram graph of the dumbbell reflects the incomplete contraction on the left side of the contracted dumbbell point cloud. Here, we assume only the peaks of the frequency that drop off on both sides by at least 2% of the number of the point samples are meaningful, as there might be surface normal vector estimation errors and data noises. Regarding the distribution of the egg tart, the multiple spikes of the contracted surfaces are also reflected as peaks on the histogram. As for the skateboard, carrot, and horse, the histograms are closer to 0.5 on average and more symmetric in comparison to other objects, aligning with their better contraction results. It is important to note the presence of normal vector differences in skeleton surfaces, leading to variations in distributions and resulting in multiple peaks in histograms. These differences could provide valuable insights into the topology of the contracting surface, such as the segments that are contracted improperly.

Since the curve skeletons are derived from the contraction results while using the Laplacian-based skeletonisation method, the quality of the resultant curve skeletons is heavily dependent on the outcomes of the contraction. Therefore, the patterns of geometric changes observed during the contraction process effectively reflect the performance of the resultant curve skeletons. As illustrated in Fig. 5. The curve skeletons generated for objects such as the hammer, skateboard, carrot, and horse exhibit the highest quality, consistent with the quality of the contraction results. In contrast, the curve skeletons generated for the cabinet, egg tart, and watermelon lack significant topological information about the object shape, mirroring the deficiencies observed in the contraction process. Besides, the observed incomplete contraction handling of the dumbbell object is reflected in the curve skeleton results as well as the bifurcation at the undesirable position.

Additionally, we applied these findings to GLSkeleton approach [26], which selectively reduces the points while shrinking the point cloud. As points are removed by the algorithm iteratively, and the mentioned differences are computed point-wise, we decide to use only the points that are consistently retained throughout the iterations for contraction pattern analysis. As illustrated in Fig. 6, similar patterns are demonstrated by the results of the contraction process of GLSkeleton. It means that the surface skeletons generated by GLSkeleton hold similar performance which confirms our propositions.

Overall, the stable convergence of the contraction and the Laplacian-based curve skeletonisation process are decided by the distributions of the curvature differences and the surface normal vector differences and their changes within
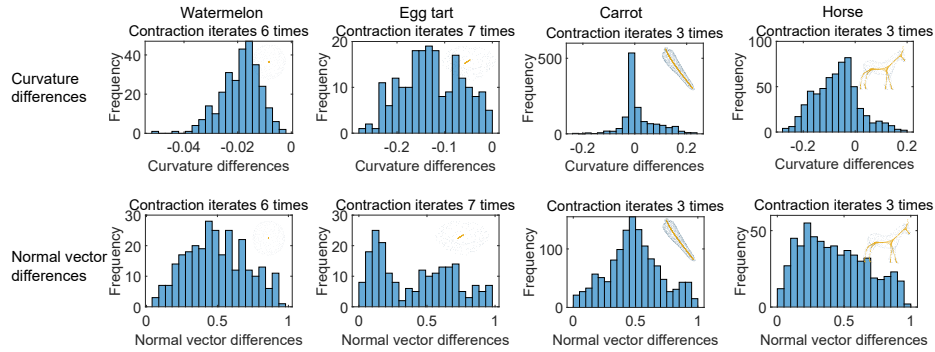
Fig. 6: Curvature vector and normal differences between the input and point cloud after contraction by GLSkeleton method. The original point cloud (grey) with the contraction results (yellow) are put at the top right corner of each histogram.

the contraction iteration. Besides, with the control by the contraction and attraction weights of Laplacian-based contraction, the distribution patterns can be corrected within the contraction process.

4   Conclusions

This work presents how we can determine whether skeletonisation by contraction methods e.g., Laplacian-based contraction can be understood about stable convergence. To develop our new proposition, we demonstrate the pattern of characteristics of curvature and normal vector changes during stable contraction and provide explanations. It is noteworthy that the defined metrics, surface normal vector and curvature difference changes, illustrate the correction of stability of contraction. However, the distribution pattern remains hypothetical and requires further quantitative analysis before we can establish a clear definition of high-quality skeleton.

In the future, we will concentrate on developing a robust framework for quantitatively analyzing changes in geometric properties. Our goal is to establish a comprehensive definition of high-quality skeleton and stable convergence of contraction for both surface skeletons and curve skeletons.

References

1. Amenta, N., Bern, M.: Surface reconstruction by voronoi filtering. In: Proceedings of the fourteenth annual symposium on Computational geometry. pp. 39–48 (1998)
2. Amenta, N., Choi, S., Kolluri, R.K.: The power crust. In: Proceedings of the sixth ACM symposium on Solid modeling and applications. pp. 249–266 (2001)
3. Arcelli, C., Di Baja, G.S., Serino, L.: Distance-driven skeletonization in voxel images. IEEE Transactions on Pattern Analysis and Machine Intelligence **33**(4), 709–720 (2010)

4. Au, O.K.C., Tai, C.L., Chu, H.K., Cohen-Or, D., Lee, T.Y.: Skeleton extraction by mesh contraction. ACM Trans. Graph. **27**(3), 1–10 (2008)
5. Cao, J., Tagliasacchi, A., Olson, M., Zhang, H., Su, Z.: Point Cloud Skeletons via Laplacian Based Contraction. In: 2010 Shape Modeling International Conference. pp. 187–197 (Jun 2010)
6. Chazal, F., Lieutier, A.: The "λ-medial axis". Graphical models **67**(4), 304–331 (2005)
7. Cornea, N., Demirci, M., Silver, D., Shokoufandeh, Dickinson, S., Kantor, P.: 3d object retrieval using many-to-many matching of curve skeletons. In: International Conference on Shape Modeling and Applications 2005 (SMI' 05). pp. 366–371 (2005)
8. Cornea, N., Silver, D., Min, P.: Curve-skeleton applications. In: VIS 05. IEEE Visualization, 2005. pp. 95–102 (2005)
9. Cornea, N.D., Silver, D., Min, P.: Curve-Skeleton Properties, Applications, and Algorithms. IEEE Trans. Vis. Comput. Graph. **13**(3), 530–548 (May 2007)
10. Giesen, J., Miklos, B., Pauly, M., Wormser, C.: The scale axis transform. In: Proceedings of the twenty-fifth annual symposium on Computational geometry. pp. 106–115 (2009)
11. Huang, H., Wu, S., Cohen-Or, D., Gong, M., Zhang, H., Li, G., Chen, B.: L1-medial skeleton of point cloud. ACM Trans. Graph. **32**(4) (jul 2013)
12. Lin, C., Li, C., Liu, Y., Chen, N., Choi, Y.K., Wang, W.: Point2skeleton: Learning skeletal representations from point clouds. In: Proceedings of the IEEE/CVF Conference on Computer Vision and Pattern Recognition (CVPR). pp. 4277–4286 (June 2021)
13. Meyer, L., Gilson, A., Scholz, O., Stamminger, M.: Cherrypicker: Semantic skeletonization and topological reconstruction of cherry trees. In: Proceedings of the IEEE/CVF Conference on Computer Vision and Pattern Recognition. pp. 6243–6252 (2023)
14. Pokorny, F.T., Stork, J.A., Kragic, D.: Grasping objects with holes: A topological approach. In: 2013 IEEE international conference on robotics and automation. pp. 1100–1107. IEEE (2013)
15. Przybylski, M., Asfour, T., Dillmann, R.: Unions of balls for shape approximation in robot grasping. In: 2010 IEEE/RSJ International Conference on Intelligent Robots and Systems. pp. 1592–1599 (2010)
16. Przybylski, M., Asfour, T., Dillmann, R.: Planning grasps for robotic hands using a novel object representation based on the medial axis transform. In: 2011 IEEE/RSJ International Conference on Intelligent Robots and Systems. pp. 1781–1788 (2011)
17. Przybylski, M., Wächter, M., Asfour, T., Dillmann, R.: A skeleton-based approach to grasp known objects with a humanoid robot. In: 2012 12th IEEE-RAS International Conference on Humanoid Robots (Humanoids 2012). pp. 376–383. IEEE (2012)
18. Qin, H., Han, J., Li, N., Huang, H., Chen, B.: Mass-driven topology-aware curve skeleton extraction from incomplete point clouds. IEEE Trans. Vis. Comput. Graph. **26**(9), 2805–2817 (2020)
19. Rezanejad, M., Samari, B., Rekleitis, I., Siddiqi, K., Dudek, G.: Robust environment mapping using flux skeletons. In: 2015 IEEE/RSJ International Conference on Intelligent Robots and Systems (IROS). pp. 5700–5705 (2015). https://doi.org/10.1109/IROS.2015.7354186
20. Saha, P.K., Borgefors, G., di Baja, G.S.: A survey on skeletonization algorithms and their applications. Pattern recognition letters **76**, 3–12 (2016)

21. Sobiecki, A., Jalba, A., Telea, A.: Comparison of curve and surface skeletonization methods for voxel shapes. Pattern Recognition Letters **47**, 147–156 (2014)
22. Stork, J.A., Pokorny, F.T., Kragic, D.: A topology-based object representation for clasping, latching and hooking. In: 2013 13th IEEE-RAS International Conference on Humanoid Robots (Humanoids). pp. 138–145. IEEE (2013)
23. Tagliasacchi, A., Delame, T., Spagnuolo, M., Amenta, N., Telea, A.: 3d skeletons: A state-of-the-art report. In: Computer Graphics Forum. vol. 35, pp. 573–597. Wiley Online Library (2016)
24. Tagliasacchi, A., Zhang, H., Cohen-Or, D.: Curve skeleton extraction from incomplete point cloud. ACM Trans. Graph. **28**(3), 1–9 (Jul 2009)
25. Vahrenkamp, N., Koch, E., Waechter, M., Asfour, T.: Planning high-quality grasps using mean curvature object skeletons. IEEE Robot. Autom. Lett. **3**(2), 911–918 (2018)
26. Wen, Q., Tafrishi, S.A., Ji, Z., Lai, Y.K.: Glskeleton: A geometric laplacian-based skeletonisation framework for object point clouds. IEEE Robotics and Automation Letters pp. 1–7 (2024). https://doi.org/10.1109/LRA.2024.3384128
27. Wu, L., Falque, R., Perez-Puchalt, V., Liu, L., Pietroni, N., Vidal-Calleja, T.: Skeleton-based conditionally independent gaussian process implicit surfaces for fusion in sparse to dense 3d reconstruction. IEEE Robot. Autom. Lett. **5**(2), 1532–1539 (2020)
28. Wu, S., Wen, W., Xiao, B., Guo, X., Du, J., Wang, C., Wang, Y.: An accurate skeleton extraction approach from 3D point clouds of maize plants. Frontiers in plant science **10**, 248 (2019)
29. Wu, T., Zhang, J., Fu, X., Wang, Y., Ren, J., Pan, L., Wu, W., Yang, L., Wang, J., Qian, C., Lin, D., Liu, Z.: Omniobject3d: Large-vocabulary 3D object dataset for realistic perception, reconstruction and generation. In: Proceedings of the IEEE/CVF Conference on Computer Vision and Pattern Recognition (CVPR). pp. 803–814 (June 2023)
30. Xia, P., Zhang, L., Li, F.: Learning similarity with cosine similarity ensemble. Information sciences **307**, 39–52 (2015)